

# PCCP

Accepted Manuscript



This is an *Accepted Manuscript*, which has been through the Royal Society of Chemistry peer review process and has been accepted for publication.

*Accepted Manuscripts* are published online shortly after acceptance, before technical editing, formatting and proof reading. Using this free service, authors can make their results available to the community, in citable form, before we publish the edited article. We will replace this *Accepted Manuscript* with the edited and formatted *Advance Article* as soon as it is available.

You can find more information about *Accepted Manuscripts* in the [Information for Authors](#).

Please note that technical editing may introduce minor changes to the text and/or graphics, which may alter content. The journal's standard [Terms & Conditions](#) and the [Ethical guidelines](#) still apply. In no event shall the Royal Society of Chemistry be held responsible for any errors or omissions in this *Accepted Manuscript* or any consequences arising from the use of any information it contains.

# Cation-exchanged SAPO-34 for adsorption-based hydrocarbon separations: Predictions from dispersion-corrected DFT calculations

*Michael Fischer<sup>+</sup>, Robert G. Bell\**

*Department of Chemistry, University College London, 20 Gordon Street, London WC1H 0AJ*

*\* Corresponding author: r.g.bell@ucl.ac.uk*

## Abstract

The influence of the nature of the cation on the interaction of the silicoaluminophosphate SAPO-34 with small hydrocarbons (ethane, ethylene, acetylene, propane, propylene) is investigated using periodic density-functional theory calculations including a semi-empirical dispersion correction (DFT-D). Initial calculations are used to evaluate which of the guest-accessible cation sites in the chabazite-type structure is energetically preferred for a set of ten cations, which comprises four alkali metals ( $\text{Li}^+$ ,  $\text{Na}^+$ ,  $\text{K}^+$ ,  $\text{Rb}^+$ ), three alkaline earth metals ( $\text{Mg}^{2+}$ ,  $\text{Ca}^{2+}$ ,  $\text{Sr}^{2+}$ ), and three transition metals ( $\text{Cu}^+$ ,  $\text{Ag}^+$ ,  $\text{Fe}^{2+}$ ). All eight cations that are likely to be found at the SII site (centre of a six-ring) are then included in the following investigation, which studies the interaction with the hydrocarbon guest molecules. In addition to the interaction energies, some trends and peculiarities regarding the adsorption geometries are analysed, and electron density difference plots obtained from the calculations are used to gain insights into the dominant interaction types. While electrostatic and polarisation effects dominate for the main group cations, significant orbital interactions are observed for unsaturated hydrocarbons interacting with transition metal cations. The differences between the interaction energies obtained for pairs of hydrocarbons of interest (such as ethylene/ethane and propylene/propane) deliver some qualitative insights: If this energy difference is large, it can be expected that the material will exhibit a high selectivity in the adsorption-based separation of alkene/alkane mixtures, which constitutes a problem of considerable industrial relevance. While the calculations show that TM-exchanged SAPO-34 materials are likely to exhibit a very high preference for alkenes over alkanes, the strong interaction may render an application in industrial processes impractical due to the large amount of energy required for regeneration. In this respect, SAPOs exchanged with alkaline earth cations could provide a better balance between selectivity and energy cost of regeneration.

+ **Current address:** Fachbereich Geowissenschaften, Universität Bremen, Klagenfurter Straße, 28359 Bremen, Germany

## Introduction

The separation of gas mixtures using adsorption-based processes, such as pressure swing adsorption (PSA) and temperature swing adsorption (TSA), has been proposed as an energy-efficient alternative to more conventional separation technologies, particularly cryogenic distillation.<sup>1</sup> Possible applications of interest include the removal of carbon dioxide from exhaust gases,<sup>2,3</sup> the separation of mixtures of light alkanes and alkenes (ethylene/ethane, propylene/propane), where a distillation process is rather inefficient due to the similar boiling points,<sup>4</sup> and the removal of acetylene impurities from an ethylene feed. Among crystalline microporous materials, aluminosilicate zeolites are the most long-established group of adsorbents. Zeolites are currently used in some large-scale industrial separation processes, for example in air separation (using PSA), and in the removal of sulphur compounds (using TSA).<sup>5</sup> Since the 1980s, a variety of zeolite-like materials with non-aluminosilicate compositions have been synthesised, among them aluminophosphates (ALPOs, stoichiometry  $\text{AlPO}_4$ ) and silicoaluminophosphates (SAPOs, stoichiometry  $\text{Si}_x\text{Al}_y\text{P}_z\text{O}_2$ , typically with  $x < 0.2$ ).<sup>5,6</sup> More recently, metal-organic frameworks (MOFs) have attracted much attention, as these novel materials provide very high porosities, and permit the incorporation of functional groups into the pore wall. Their potential for gas separation has been reviewed by different authors.<sup>7,8</sup> Although some MOFs exhibit very promising properties, such as high selectivities and working capacities, their limited stability currently hampers industrial applications. Therefore, continued research efforts are dedicated to the synthesis, characterisation, and optimisation of aluminosilicate zeolites and zeolite-like materials such as ALPOs and SAPOs for gas separation processes.

A number of studies have addressed the selective adsorption of carbon dioxide in ALPOs and SAPOs. For example, Hedin and co-workers have compared the  $\text{CO}_2$  adsorption properties of (silico)aluminophosphate materials with different topologies.<sup>9,10</sup> The adsorption of  $\text{CO}_2$ ,  $\text{N}_2$ , and  $\text{CH}_4$  in cation-exchanged SAPO-34, a system with chabazite framework topology, has been studied by Rivera-Ramos et al., who reported particularly favourable properties for selective  $\text{CO}_2$  adsorption in Sr-exchanged SAPO-34.<sup>11,12</sup> Other researchers have addressed the use of the same material in membrane-based separations involving  $\text{CO}_2$ ,  $\text{CH}_4$ ,  $\text{N}_2$  and  $\text{H}_2$ .<sup>13-15</sup> In the field of alkene/alkane separation, a number of investigations have focussed on all-silica zeolites.<sup>16-18</sup> In the specific case of all-silica chabazite (Si-CHA), the hindered diffusion of propane through the eight-ring windows leads to a high selectivity based on adsorption kinetics, rather than equilibrium adsorption.<sup>17,19</sup> By comparing Si-CHA to the isostructural systems ALPO-34 and SAPO-34, it was shown that the diffusivity of propane through these chabazite-type structures is strongly influenced by small changes in the window diameter.<sup>4</sup> A later study confirmed SAPO-34 as a promising material for propylene/propane separation.<sup>20</sup> Regarding zeolites exchanged with main group cations, most studies have focussed on commercially produced materials, primarily zeolites A and X. For example, a comparative investigation revealed that zeolite 4A, 5A and faujasite-type zeolite 13X exhibit very

similar equilibrium selectivities in ethylene/ethane separation, despite their widely differing pore diameters.<sup>4</sup> The use of zeolites exchanged with transition metal (TM) cations, especially  $\text{Cu}^+$  and  $\text{Ag}^+$ , has been proposed to enhance the selectivity, as these cations interact strongly with unsaturated hydrocarbons.<sup>21–23</sup> A strong orbital interaction between TM cations and the  $\pi$ -system of unsaturated hydrocarbons has also been observed in other adsorbents, such as mesoporous materials loaded with copper or silver cations (“ $\pi$ -complexing sorbents”),<sup>24–26</sup> and in metal-organic frameworks containing coordinatively unsaturated metal sites.<sup>27–30</sup>

Computational methods can be used as a complement to experimental studies, either to predict the properties of new or uncharacterised materials, or to enhance the understanding of known systems. For example, force-field based simulations have been used in large-scale screening studies to predict the  $\text{CO}_2/\text{N}_2$  and ethylene/ethane selectivity of a large number of zeolite frameworks,<sup>31,32</sup> and in smaller-scale investigations aimed at a better understanding of the relationships between topology and adsorption properties.<sup>33,34</sup> While this type of calculation requires an adequate set of predefined parameters to represent interatomic interactions, electronic structure methods, such as density-functional theory (DFT), can deliver first-principles insights into the interactions that govern adsorption. A particular aspect that needs to be considered is the importance of dispersion interactions, which are not properly accounted for in standard DFT calculations, but need to be included to obtain reasonably accurate adsorption energies for most guest molecules. The adsorption of alkanes, which interact primarily through dispersion interactions, has been used as a model case to compare different dispersion correction schemes, both for proton-exchanged and cation-exchanged chabazites.<sup>35,36</sup> The adsorption of alkenes and alkynes has been primarily studied in TM-exchanged zeolites, where electronic structure methods can provide insights into the orbital interactions between the cation and the adsorbed species.<sup>37–40</sup>

Materials with the chabazite topology, such as SAPO-34, hold considerable promise for applications, and systems incorporating a variety of cations have been synthesised. Moreover, the unit cell is relatively small, and there are only a limited number of cation sites that need to be considered. For all these reasons, SAPO-34 is a well-suited model system for a systematic computational investigation that aims to elucidate the impact of the cation on the interaction with different hydrocarbon species. In this study, we present results of dispersion-corrected DFT calculations for a total of five different hydrocarbons ( $\text{C}_2\text{H}_6$ ,  $\text{C}_3\text{H}_8$ ,  $\text{C}_2\text{H}_4$ ,  $\text{C}_3\text{H}_6$ ,  $\text{C}_2\text{H}_2$ ) adsorbed at the cation sites of X-SAPO-34, with X representing a total of eight different cations ( $\text{Li}^+$ ,  $\text{Na}^+$ ,  $\text{Mg}^{2+}$ ,  $\text{Ca}^{2+}$ ,  $\text{Sr}^{2+}$ ,  $\text{Cu}^+$ ,  $\text{Ag}^+$ ,  $\text{Fe}^{2+}$ ). After analysing interaction energies and adsorption geometries, the DFT electron density difference is exploited to gain insights into the nature of the cation-guest interaction for cases of special interest. Finally, we use the DFT results to draw some conclusions regarding the materials’ suitability for hydrocarbon separation applications. Due to the dominant role of the cation, we expect that the

qualitative findings are to some extent transferable to other SAPOs and zeolites in which the cations occupy a similar environment.

## Models and methods

### Computational details

The DFT calculations were carried out using the CASTEP code, which employs a plane wave basis set and pseudopotentials.<sup>41</sup> The calculations used the PBE exchange-correlation functional in conjunction with Grimme-type dispersion corrections (PBE-D2),<sup>42,43</sup> and employed ultrasoft pseudopotentials and a plane wave cutoff of 380 eV. Only the gamma point was used to sample the Brillouin zone, after establishing that the use of a larger k-mesh ( $2 \times 2 \times 2$  k-points) does not change the results significantly. Spin-polarised calculations were carried out for the case of Fe-SAPO-34.

In the calculations, the Grimme-type D2 dispersion correction was employed to account for dispersion interactions.<sup>43</sup> It has been established that more sophisticated methods, such as the DFT/CC scheme or the random-phase approximation, which have been used for some guest molecules in cation-exchanged zeolites, are able to provide results of superior quality.<sup>35,36,44</sup> In this work, however, it is our primary aim to study a relatively large set of cations and different hydrocarbon guest species on an equal footing. Such computations would be prohibitively expensive if the aforementioned methods were used. As all results are obtained with the same methodological approach, we can directly compare the interaction energies calculated for different systems, enabling us to comment on the potential of cation-exchanged chabazite-type SAPOs for the separation of mixtures of small hydrocarbons. Nevertheless, it is apparent that the DFT-D method, which uses empirical dispersion coefficients that are independent of the chemical environment, has inherent limitations which have been discussed elsewhere.<sup>45,46</sup> Therefore in the future it would be worthwhile to study the most promising systems using more accurate computational methods.

### Structural model of SAPO-34

All calculations were carried out using the rhombohedral representation of the unit cell of SAPO-34. The lattice parameters of SAPO-34 were taken from the work of Leardini et al., and were held fixed in the calculations ( $a = 9.373 \text{ \AA}$ ,  $\alpha = 94.7286 \text{ deg}$ ).<sup>47</sup> The calculations without guest molecules were performed in space groups  $P-1$  or  $PI$ , and all calculations with adsorbed molecules were carried out in  $PI$ . The Si/P ratio of the model system was taken to be 1/2. The question of the silicon distribution in

SAPOs is one of particular relevance, and phenomena such as “silicon island formation” have been investigated in detail.<sup>48</sup> As this is not a central question of this study, however, we arbitrarily place the framework silicon atoms at opposite vertices of a double six-ring unit (figure 1(b)). The complete unit cell of the model system contains 24 oxygen, 6 aluminium, 4 phosphorous, and 2 silicon atoms, and the charge of the framework is compensated by either two monovalent or one divalent cation per cell. As a representative of the model system used in the calculations, the complete unit cell of Na-*SAPO*-34 is visualised in the Electronic Supplementary Information (figure S1).

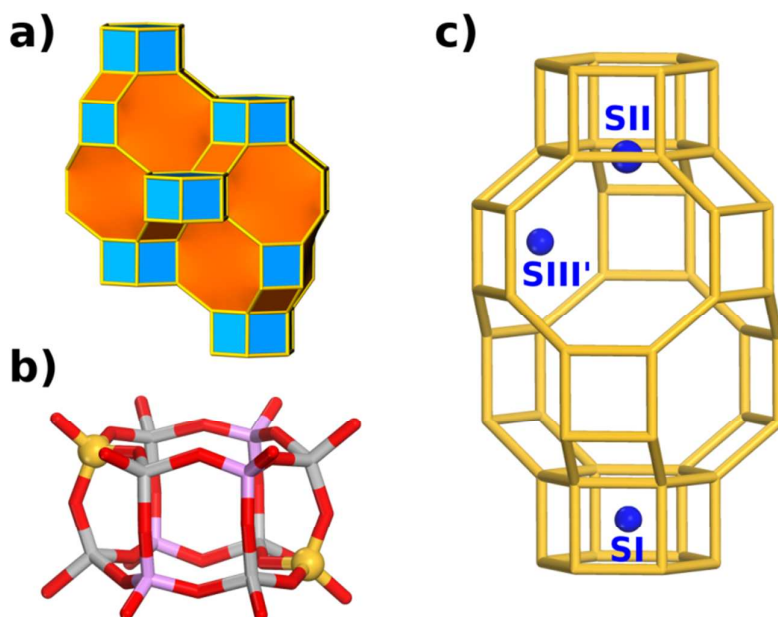


Figure 1: a) Visualisation of the building blocks of the chabazite structure, with double six-ring (d6R) units shown in blue, and chabazite cages in orange. b) Atomistic representation of a d6R unit of SAPO-34 as used in the calculations: Grey = aluminium, violet = phosphorous, yellow = silicon, red = oxygen. c) Schematic representation of cation sites in SAPO-34, showing one chabazite cage and two d6R units.

## Results and discussion

### Preferred cation sites

There are a variety of possible cation sites in the chabazite structure. The relevant sites are shown in figure 1(c), with the nomenclature following the work of Smith et al.<sup>49</sup> Site SI is located at the centre of the double six-ring (d6R) unit. As this site is fully surrounded by framework atoms, the cation has

limited possibilities to interact with guest molecules. Therefore, site SI is not considered in this work. Site SII is located at the centre of the six-ring, while site SIII' is located at the centre of the eight-ring windows (SIII designates the position above one four-ring, while SIII' is displaced towards the centre of the eight-ring).<sup>50</sup> To determine the site preferences of the different cations, DFT-D geometry optimisations were carried out for two separate cases, with the cations at site II, or at site III', respectively. For each cation, the energy difference  $\Delta E(\text{SII-SIII}')$  was then calculated. The results are summarised in figure 2 (and table S1), and the optimised geometries are visualised in the ESI.

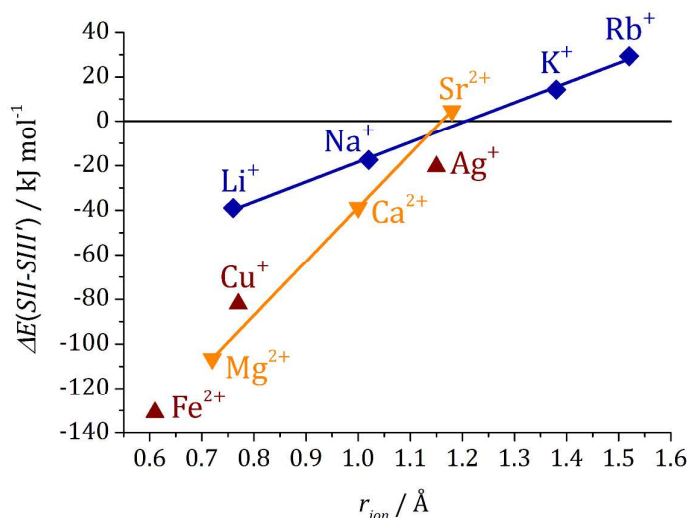


Figure 2: Plot of the energy difference  $\Delta E(\text{SII-SIII}')$  against the ionic radius.<sup>51</sup> The energy difference is calculated per cation, rather than per unit cell. Linear fits are included for the alkali metals and the alkaline earth metals.

For the monovalent cations, site SII is favoured for the smaller alkali cations (Li and Na) and the transition metals (TM) considered (Cu and Ag), while the larger alkali cations K and Rb prefer the SIII' site. For the alkali cations (and, separately, for the alkaline earth cations, *vide infra*), a near-perfect correlation between the ionic radius and the energy difference  $\Delta E(\text{SII-SIII}')$  can be established (figure 2). Although the TM cations are scattered around the trendline, the correlation suggests that monovalent cations with a radius below approximately 1.2 Å are small enough to be accommodated at the SII site. A number of experimental studies addressing the siting of alkali cations in chabazite-type structures have been published, especially for aluminosilicate chabazite. There is clear evidence that Li prefers the SII site, while K occupies the SIII' site, in line with our observations.<sup>49,52</sup> Sodium appears to be preferred at the SIII' site at low loadings, but it tends to occupy the SII site in systems

with high sodium content, or in the presence of potassium.<sup>52,53</sup> Previous computational studies of chabazite by Civalleri and co-workers, as well as our own previous work, have reported the same trend as the present study.<sup>50,54</sup>

The silver cations in Ag-SAPO-34 are located in a very similar position to the sodium cations in the Na-containing system, centrally above the six-ring. Experimentally, occupation of this site, as well as of sites SI and SIII', was observed in a fully exchanged sample of Ag-chabazite, which has a much higher cation content.<sup>55</sup> The result obtained for Cu-SAPO-34 deserves a more detailed discussion. As in the cases of Li, Na, and Ag, the Cu cations are located near the centre of the six-ring. While the other cations are displaced into the chabazite cage, with the magnitude of the displacement correlating with the ionic radius, the Cu cations are displaced towards the interior of the double six-ring. This leads to a very short Cu-Cu distance of 2.55 Å (figure S9). Clearly, such a short distance between the Cu(I) centres is indicative of a significant copper-copper interaction. Evidence for Cu<sub>2</sub><sup>2+</sup> dimers has been obtained in previous experimental and theoretical studies, especially for Cu-ZSM-5, where they are believed to play an important role in nitric oxide decomposition: Here, previous DFT investigations predicted similarly short Cu<sup>+</sup>-Cu<sup>+</sup> distances of about 2.5 Å for some cases.<sup>56,57</sup> The detailed computational study of Cu-chabazite by Göttl et al. also revealed a preference of Cu<sup>+</sup> (and Cu<sup>2+</sup>, in line with experimental results<sup>58,59</sup>) for the SII site.<sup>60</sup> However, the aspect of dimer formation was not investigated in that work, which considered a smaller number of cations per cell. In general, we can expect that the formation of a Cu<sub>2</sub><sup>2+</sup> dimer will have an impact on the interaction with adsorbed species. As the focus of our study is the behaviour of single cations, rather than dimeric units, we chose to use a different model system to analyse the interaction with copper. This system includes one Cu and one Na cation per d6R unit, precluding the formation of Cu<sub>2</sub><sup>2+</sup> dimers. Five different possible cation distributions between sites I, II, and III', were considered (see Supp. Inf.), and it was found that the system with both cations at the SII site is the energetically most stable arrangement. Compared to the dimer-containing Cu-SAPO-34, the Cu cation is displaced towards the chabazite cage in Cu/Na-SAPO-34, and it forms short bonds to the three surrounding oxygens (bond lengths between 1.92 and 2.12 Å). In the following, all results involving copper were obtained for this system. As a final remark, it should be pointed out that Cu<sup>+</sup>/Cu<sup>2+</sup> cations in zeolites are susceptible to oxidation/reduction, which may render both oxidation states relevant for some applications.<sup>60,61</sup> However, the present study focusses exclusively on monovalent copper cations, which can be obtained by autoreduction of Cu<sup>2+</sup> cations at high temperature.

Calculations for systems incorporating divalent cations used the same number of Si atoms per cell as described above. Therefore, only one cation per cell is required to balance the negative framework charge. For Mg, Ca, and Fe(II), the site associated with the six-ring is always significantly favoured over the site associated with the eight-ring window. Both cation sites are very close in energy in Sr-SAPO-34. While the larger cations Ca and Sr are located centrally above the six-ring, Mg and Fe are

slightly displaced from the centre, forming close contacts with framework oxygens that neighbour the silicon atom (figures S6 and S11). It is significant that the plot of  $\Delta E(\text{SII-SIII}')$  against ionic radius for the three alkaline earth cations shows a linear correlation, in line with the observation made above for the alkali cations. The 1.16 Å “threshold” radius, i.e. the ionic radius above which site SIII' is favoured, derived from this correlation is only slightly smaller than the corresponding value for the alkali cations ( $\sim 1.2$  Å).

The interaction of a guest molecule with a cation will depend to some extent on the cation site, and we have addressed this issue for selected cases in chabazite in previous work.<sup>54</sup> However, a complete investigation of the impact of the cation site is beyond the scope of this study, where it is our primary aim to investigate the influence of the nature of the cation on the interaction with adsorbed molecules in a comparable environment. For the remainder of this work, we will focus exclusively on systems in which cations are located at the SII site. We thus consider all cations for which the SII site is energetically preferred location, and include strontium as a borderline case due to the very small positive value of  $\Delta E(\text{SII-SIII}')$ .

### Interaction with adsorbed molecules: Ethane and propane

For ethane and propane, two different orientations were considered in the DFT starting geometries: A side-on orientation, in which the hydrocarbon approaches the cation with a C-C bond perpendicular to the cation-hydrocarbon axis, and an end-on orientation, in which the C-C bond is oriented parallel to this axis. With the exception of  $\text{C}_3\text{H}_8$  in of Fe-SAPO-34, where the end-on configuration is favoured by less than 1  $\text{kJ mol}^{-1}$ , the side-on orientation is always the preferred orientation, with energy differences between the two orientations ranging from virtually zero to approximately 10  $\text{kJ mol}^{-1}$ . Only the results for the side-on orientation, which are given in tables 1 and 2, respectively, are discussed in the following.

In all systems, the interaction with propane is distinctly stronger than with ethane, with the difference ranging from -8 to -18  $\text{kJ mol}^{-1}$ . It is straightforward to attribute this behaviour to increased dispersive interactions with the larger propane molecule. This intuitive explanation is supported by the fact that the largest differences are observed in systems with heavy cations, especially Sr-SAPO-34 and Ag-SAPO-34. Furthermore, it can be substantiated by comparing the interaction energy  $E_{int}$  obtained from dispersion-corrected DFT to a “DFT-only” energy  $E_{nodisp}$ , where the dispersion term is subtracted. The values of  $E_{nodisp}$  are listed in the ESI (tables S2 and S3), and they are very similar for ethane and propane for all systems. Comparing the different groups of cations, the systems incorporating alkaline

earth metals interact most strongly with both molecules, with interaction energies around  $-70 \text{ kJ mol}^{-1}$  for ethane, and reaching nearly  $90 \text{ kJ mol}^{-1}$  for propane. The interaction in the TM-containing systems is typically weaker than in the alkali-exchanged SAPOs, with the exception of propane in Ag-SAPO-34. For SAPOs containing main group cations, the distances between the cations and the alkane molecules evolve more or less in accordance with the ionic radii, with the exception of the peculiar case of propane in Mg-SAPO-34, which will be discussed below. On the other hand, the distances of TM cations to the guest molecules are rather large, exceeding  $3.0 \text{ \AA}$  in all cases.

Table 1: DFT interaction energies  $E_{int}$  and equilibrium distances  $d(\text{cation-c.o.m.})$  (with c.o.m. being the centre of mass of the hydrocarbon) for ethane, ethylene, and acetylene.

	$\text{C}_2\text{H}_6$		$\text{C}_2\text{H}_4$		$\text{C}_2\text{H}_2$	
	$E_{int} / \text{kJ mol}^{-1}$	$d(M\text{-c.o.m.}) / \text{\AA}$	$E_{int} / \text{kJ mol}^{-1}$	$d(M\text{-c.o.m.}) / \text{\AA}$	$E_{int} / \text{kJ mol}^{-1}$	$d(M\text{-c.o.m.}) / \text{\AA}$
Li-SAPO-34	-57.9	2.46	-66.6	2.33	-65.1	2.34
Na-SAPO-34	-57.2	2.68	-61.6	2.66	-57.3	2.68
Mg-SAPO-34	-72.0	2.62	-102.0	2.44	-98.2	2.43
Ca-SAPO-34	-72.3	2.83	-84.9	2.82	-82.6	2.79
Sr-SAPO-34	-67.2	2.99	-80.5	3.02	-75.5	3.03
Cu/Na-SAPO-34	-39.5	3.25	-165.7	1.86	-151.7	1.83
Ag-SAPO-34	-49.6	3.04	-128.4	2.16	-106.5	2.16
Fe-SAPO-34	-37.7	3.27	-168.0	1.88	-149.5	1.86

Table 2: DFT interaction energies  $E_{int}$  and equilibrium distances  $d(\text{cation-c.o.b.})$  (with c.o.b. being the centre of the closest C-C bond of the hydrocarbon) for propane and propylene.

	$\text{C}_3\text{H}_8$		$\text{C}_3\text{H}_6$	
	$E_{int} / \text{kJ mol}^{-1}$	$d(M\text{-c.o.b.}) / \text{\AA}$	$E_{int} / \text{kJ mol}^{-1}$	$d(M\text{-c.o.b.}) / \text{\AA}$
Li-SAPO-34	-65.5	2.40	-84.2	2.35
Na-SAPO-34	-69.3	2.67	-81.7	2.67
Mg-SAPO-34	-86.4	2.98	-127.5	2.44
Ca-SAPO-34	-88.3	2.82	-111.3	2.77
Sr-SAPO-34	-85.7	3.01	-112.4	2.95
Cu/Na-SAPO-34	-52.3	3.26	-175.9	1.88
Ag-SAPO-34	-66.0	3.06	-145.0	2.17
Fe-SAPO-34	-50.0	3.37	-182.4	1.89

To investigate the interaction between propane and the framework more closely, the electron density differences obtained from the DFT calculations were visualised for Li-SAPO-34, Mg-SAPO-34, Cu/Na-SAPO-34, and Fe-SAPO-34 (figure 3; analogous plots for ethane, which are qualitatively very similar, are shown in the ESI). To calculate this difference, the guest molecule and the framework are defined as distinct fragments, and separate DFT calculations are carried out for each fragment. The density difference is then obtained by subtracting the electron density of the fragments from that of the combined system. The plots for Li-SAPO-34 and Mg-SAPO-34 show a significant rearrangement of the alkane electron density due to interaction with the cation. In the Li-exchanged system, electrons accumulate between the cation and the C-C bond of the guest molecule, while the electron density at the alkane hydrogen atoms is reduced. A qualitatively similar, but more pronounced rearrangement is observed in Mg-SAPO-34. This indicates that polarisation interactions are stronger in this case, a behaviour that is not surprising given the increased polarising power of the divalent cation. Since electrostatic interactions with the alkanes, especially with ethane, are generally weak, the increased polarisation interactions are the main factor contributing to the stronger total interaction in systems containing alkaline earth cations when compared to their alkali-exchanged counterparts. In the case of propane in Mg-SAPO-34, the  $C_3H_8$  molecule rotates, coordinating to the cation via the central carbon atom. This nearly symmetric arrangement appears energetically more favourable than coordination via a single C-C bond, when the polarising power of the cation is high enough. Considering the TM-exchanged systems, the plot for Cu/Na-SAPO-34 indicates only very weak polarisation of the alkane molecule, in line with the reduced interaction strength in this system. A significantly different picture emerges for Fe-SAPO-34, although it might be expected that this system would behave in a similar way to the copper-containing SAPO. Here, the most notable feature is a dramatic change in electron density at the cation site, and near the framework oxygens surrounding the cation. While there are no indications of an appreciable charge transfer, it seems that a significant rearrangement of electrons in the  $d$ -orbitals of the  $Fe^{2+}$  cation occurs, which is most likely caused by repulsion arising from the presence of the propane molecule in close proximity to the cation. However, the rearrangement does not lead to a change in spin state, and the  $Fe^{2+}$  cation remains in the high-spin state.

Before comparing the results of our study to previous computational and experimental results, it is useful to highlight some general aspects. Throughout this work, we refer to the interaction energy, which is directly taken from the DFT calculations. This can be compared to analogous energy values from previous computational studies. However, the comparison with experimental data is hampered by the fact that there is no direct experimental analogue for this quantity. Instead, the isosteric heat of adsorption is an experimentally accessible measure of the strength of host-guest interactions. (NB: The isosteric heat, which is typically referred to as  $q_{st}$ , is positive by definition.). Direct computational predictions of the isosteric heat are possible, but demanding, due to the necessity to include

vibrational contributions. Furthermore, it would be necessary to account for different possible locations of the guest molecule in the pores of the adsorbent. Among others, Nachtigall and co-workers and Pirngruber and co-workers have carried out detailed computations for CO<sub>2</sub> in zeolites.<sup>62,63</sup> A more approximate approach to account for temperature effects, in this instance for the case of alkanes in Na-CHA, was used by Göttl et al.<sup>35</sup> Here, the correction term to account for temperature effects amounts to roughly 10 kJ mol<sup>-1</sup> at  $T = 300$  K, with the isosteric heat of adsorption having a smaller absolute value than the uncorrected DFT energy. While a detailed treatment including vibrational corrections is beyond the scope of the present study, this previous result leads us to expect that the interaction energies should ideally exhibit semi-quantitative agreement with experimental heats of adsorption. Furthermore, qualitative trends that are observed in the DFT interaction energy should be reflected in a similar way in the isosteric heat of adsorption.

It is particularly insightful to discuss our results obtained for Na-SAPO-34 in the light of the aforementioned study of Na-CHA performed by Göttl et al.<sup>35</sup> These authors compared different means to account for dispersion interactions. Using another parameterisation of the Grimme-type correction, they obtained energies of -52.5 kJ mol<sup>-1</sup> for ethane and -64.2 kJ mol<sup>-1</sup> for propane in Na-CHA. The interaction energies predicted in our work are somewhat larger than these values. Among the other approaches tested by Göttl et al., the vdW-DF method predicted a stronger interaction, and two different implementations of the random phase approximation resulted in energies of -26.9/-33.0 kJ mol<sup>-1</sup> for ethane and -41.1/-49.8 kJ mol<sup>-1</sup> for propane. A comparison with the experimental results of Denayer and co-workers for Na-CHA, which was already included in this previous study, shows that the DFT-D calculations have a pronounced tendency to overestimate the interaction strength, since the experimental heats of adsorption amount to 34 kJ mol<sup>-1</sup> for ethane, and 47 kJ mol<sup>-1</sup> for propane.<sup>64</sup> The difference between the PBE-D2 energies and these values is too large to be explained solely by missing temperature corrections. Göttl et al. hypothesised that the double-counting of short-range exchange-correlation effects in the DFT-D and vdW-DF approaches could lie at the origin of these discrepancies.<sup>35</sup> Apart from the study by Denayer and co-workers, experimental measurements of ethane or propane in cation-exchanged chabazite-type materials are scarce.

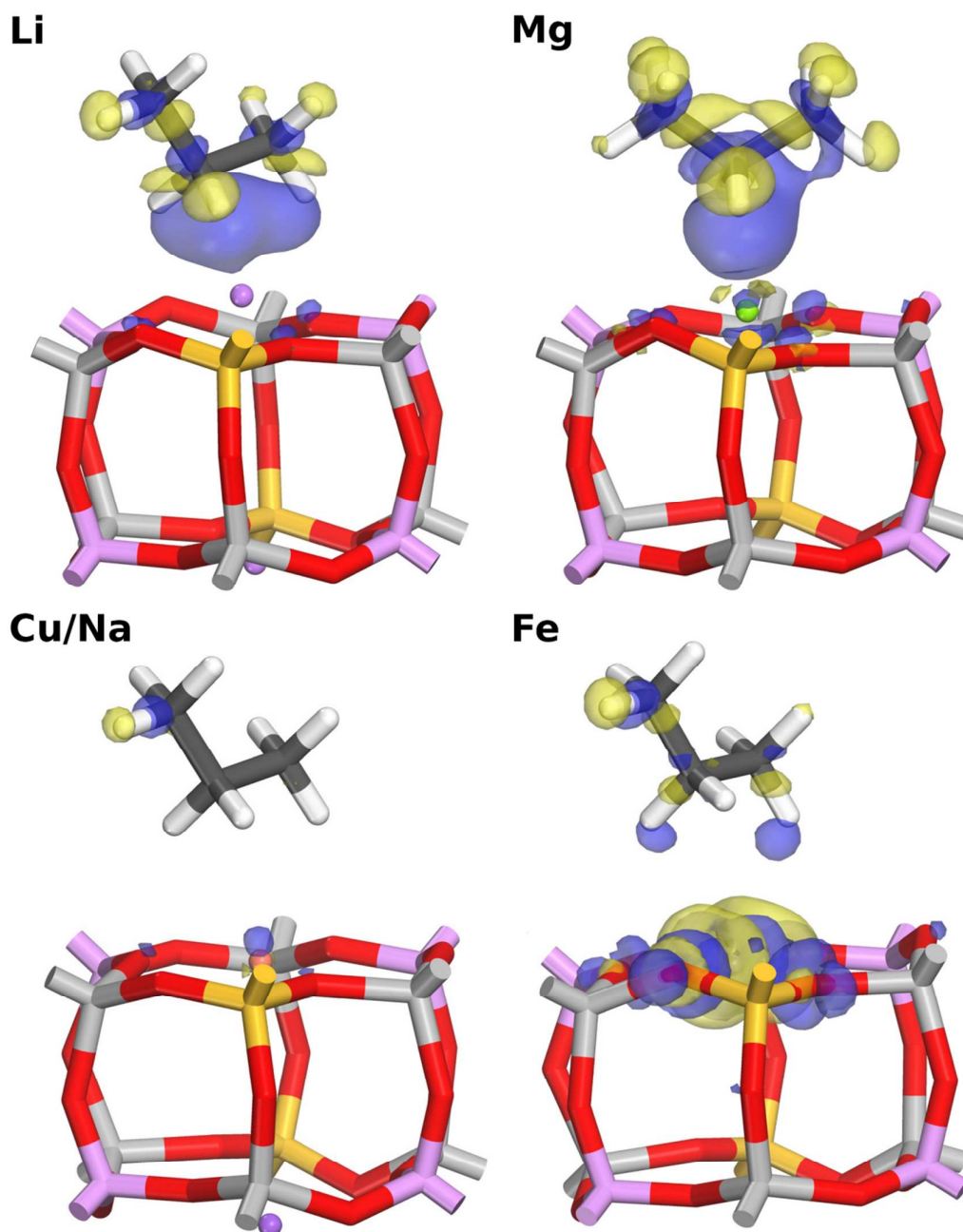


Figure 3: Isosurface of the electron density difference for propane adsorbed in Li-, Mg-, Cu/Na-, and Fe-SAPO-34. The isosurfaces were created for an isodensity value of  $0.01 \text{ e } \text{\AA}^{-3}$ . Blue designates regions of charge accumulation, and yellow designates regions of charge depletion.

**Interaction with adsorbed molecules: Ethylene, propylene, and acetylene**

For the unsaturated hydrocarbons, only the side-on orientation was considered as starting geometry. The DFT results for the three molecules are summarised in tables 1 and 2. In all systems, the interaction strength with the different guest species evolves as follows:  $C_2H_4 > C_2H_2 > C_2H_6$  and  $C_3H_6 > C_3H_8$ . However, the magnitude of the differences in energy varies widely. For the systems that contain alkali cations, the interaction with the unsaturated  $C_2$  hydrocarbons is only modestly stronger than for ethane, with the differences in interaction energy not exceeding  $8 \text{ kJ mol}^{-1}$ . An increased affinity towards the unsaturated species is observed for the propylene/propane pair, a feature that can be explained by the appreciable difference in dipole moment between the two molecules ( $d(C_3H_6) = 0.076 \text{ e \AA}$ ,  $d(C_3H_8) = 0.017 \text{ e \AA}$ ).<sup>65</sup> This trend is more pronounced in the systems containing alkaline earth cations: For Mg-SAPO-34, the interaction energies obtained for the unsaturated hydrocarbons are much larger than for the saturated species, reaching  $-127 \text{ kJ mol}^{-1}$  for propylene, and ranging near  $-100 \text{ kJ mol}^{-1}$  for the  $C_2$  species. Ca- and Sr-SAPO-34 show an intermediate behaviour, with interaction energies around  $-110 \text{ kJ mol}^{-1}$  for propylene, and about  $-80 \text{ kJ mol}^{-1}$  for ethylene and acetylene. For the latter two sorbates in the alkali-exchanged SAPOs, the distances between cation and guest molecule are quite similar for saturated and unsaturated hydrocarbons. Mg-SAPO-34 is an exception, as a rather pronounced reduction in distance occurs here. It is also worth noting that the length of the C-C bond in all systems containing main group cations does not change significantly upon adsorption, with the observed elongation never exceeding  $0.02 \text{ \AA}$ . A very large increase of the interaction strength is observed in all the TM-exchanged SAPOs: here, the interaction energies, which range between  $-107 \text{ kJ mol}^{-1}$  and  $-185 \text{ kJ mol}^{-1}$ , indicate chemisorption, rather than physisorption. Fe-SAPO-34 and Cu/Na-SAPO-34 exhibit a markedly stronger interaction than the silver-exchanged system for all guest molecules. The metal-guest distances are drastically shorter than typical non-covalent contacts, mostly falling below  $2 \text{ \AA}$ . Furthermore, the C-C double (triple) bond is elongated by up to  $0.07 \text{ \AA}$  ( $0.05 \text{ \AA}$ ) when compared to the free molecule, another feature that points towards a covalent interaction.

The electron density difference is visualised for ethylene in Li-, Mg-, Cu/Na- and Fe-SAPO-34 in figure 4. Results for propylene and acetylene are shown in the ESI (figures S14 and S15). As far as the guest molecule is concerned, the observed evolution is qualitatively similar in Li-SAPO-34 and Mg-SAPO-34. However, the magnitude of the rearrangement is considerably larger in the latter system: Electron density is removed from the hydrogen atoms, and from the regions below and above the C-C bond. An accumulation of electron density occurs in the region between the hydrocarbon and the cation. In the case of Mg-SAPO-34, there is also a slight rearrangement of electrons associated with the cation, which are displaced from the side of the guest molecule to the opposite side (towards the centre of the d6R unit). Presumably, this is related to the electrostatic repulsion arising from the polarised charge cloud of the guest molecule. As mentioned above, the contact between cation and

guest molecule is very short in this case, an observation explained by the combination of the large polarising power and relatively small van der Waals radius of the  $\text{Mg}^{2+}$  cation. There are, however, no indications of a significant charge transfer between cation and hydrocarbon molecule, in line with the common interpretation that cation- $\pi$  bonding of main group cations is dominated by electrostatic and polarisation interactions.<sup>66,67</sup>

As similar observations are made for Cu/Na-SAPO-34 and Ag-SAPO-34, only the copper-exchanged system is discussed here (density difference plots for Ag-SAPO-34 are provided in the SI). Somewhat similar to Mg-SAPO-34, the most significant increases of the electron density are observed along the C-C bond of the ethylene molecule, and in the region between the cation and the guest. The electron density is reduced above and below the C-C bond, at the sites of the hydrogen atoms, and in the direct environment of the cation. Due to the large interaction energies and short metal-guest distances, we can expect that electrostatic and polarisation interactions are complemented by orbital interactions in the TM-exchanged systems. While a detailed study of the molecular orbitals themselves is beyond the scope of this study, some conclusions can be drawn by discussing the results in the light of a previous study by Nechaev *et al.*<sup>68</sup> These authors used DFT calculations to study the interaction of  $\text{Cu}^+$ ,  $\text{Ag}^+$ , and  $\text{Au}^+$  cations with ethylene and acetylene ligands, employing energy decomposition analysis to obtain insights into the nature of the bonding. The analysis indicated a significant covalent contribution to the bonding, which accounts for slightly less than half of the total attractive interaction (the remaining part being electrostatic). Both  $\sigma$ -donation from the HOMO of the ligand to the TM and  $\pi$ -back-donation from TM d-orbitals to the ligand's LUMO play a role, with the former contributing at least twice as much to the interaction as the latter. If we attempt to interpret the electron density difference plot shown in figure 4 for Cu/Na-SAPO-34 along these lines, we can attribute the decreases in electron density in the environment of the ethylene molecule, together with the increase in the area between cation and guest molecule, as being due to  $\sigma$ -donation, while the reduction at the metal centre, together with the increase along the C-C bond, can be explained with  $\pi$ -back-donation. Furthermore, it is worth mentioning that Nechaev *et al.* found the interaction to be stronger for  $\text{Cu}^+$  than for  $\text{Ag}^+$ , and stronger for ethylene than for acetylene, in qualitative agreement with our results. In the case of Fe-SAPO-34, we observe an even more pronounced rearrangement of the electron density, the most peculiar feature being a decrease in electron density along a line connecting the cation and the centre of the C-C bond, accompanied by a very pronounced increase to both sides of this region, and close to the carbon atoms. Comparing this system to Cu/Na-SAPO-34, the observed changes may indicate that the balance between  $\sigma$ -donation and  $\pi$ -back-donation shifts towards the latter, because only  $\sigma$ -donation involves a metal orbital that points towards the centre of the C-C bond.<sup>68</sup> On the other hand, the elongation of C-C bond described above, which is another sign of  $\pi$ -back-donation, is only slightly more pronounced in the  $\text{Fe}^{2+}$ -containing system. Therefore, we cannot quantify the relative importance of donation and back-donation components on the basis of these results. Nevertheless, it is

safe to conclude that orbital interactions have a significant effect on the adsorption of unsaturated hydrocarbons in these systems. It should be noted that a considerably more detailed DFT study of ethylene and acetylene in Cu- and Ag-exchanged ZSM-5 has been reported.<sup>40</sup>

Experimental data on any of the unsaturated hydrocarbons in SAPO-34 materials or aluminosilicate chabazites are lacking, apart from the work of Agarwal et al, who investigated the kinetically based separation of propylene/propane mixtures in H-SAPO-34,<sup>20</sup> and some studies of all-silica chabazite.<sup>17,19</sup> However, due to the much stronger interaction with the cations when compared to the saturated counterparts, we can expect that the qualitative trends inferred from our work should also be observed in zeolite-like materials with other topologies. As early as 1971, Bezus et al. investigated the adsorption of ethylene in alkali-exchanged zeolite X, observing a decrease of the affinity with increasing cation radius, the difference in isosteric heat between the Li- and the Na-exchanged system amounting to roughly 10 kJ mol<sup>-1</sup>.<sup>69</sup> The absolute values (amounting to 50 kJ mol<sup>-1</sup> for the Li-exchanged system) are somewhat smaller than the DFT interaction energies obtained in the present work. In subsequent studies of Na-exchanged zeolite X, isosteric heats of adsorption between 43 and 53 kJ mol<sup>-1</sup> for propylene, and between 33 and 43 kJ mol<sup>-1</sup> for propane, were obtained.<sup>22</sup> While these values are roughly 20 to 30 kJ mol<sup>-1</sup> lower than the DFT interaction energies obtained, the typical difference between the two species is around 10 kJ mol<sup>-1</sup>, in good agreement with the value of  $\Delta E_{int}(C_3H_6-C_3H_8)$  inferred from our results (-12 kJ mol<sup>-1</sup>). The adsorption of unsaturated hydrocarbons in zeolites exchanged with alkaline earth metals has been investigated to a much lesser extent, despite rather promising early results obtained using chromatography.<sup>70</sup>

Due to their ability to strongly bind unsaturated hydrocarbons via orbital interactions, TM-exchanged systems have been studied in some detail. Pioneering work was carried out by Yang and co-workers in the field of non-zeolitic “ $\pi$ -complexing” sorbents, mainly regarding Cu- and Ag-doped amorphous materials.<sup>24,25</sup> In the field of zeolites, Aguilar-Armenta and Patino-Iglesias reported a very high heat of propylene adsorption of 91 kJ mol<sup>-1</sup> in Ag-exchanged erionite.<sup>21</sup> Doping with CuCl was found to increase the preference of zeolite X for propylene over propane; however the increase in the heat of adsorption was only moderate, indicating a much weaker interaction than in the model system studied in our work.<sup>22</sup> Recently, Aguado et al. reported a very high selectivity of silver-exchanged zeolite A for ethylene over ethane.<sup>23</sup> In addition to the preferential adsorption of ethylene over ethane, which is enhanced by exchanging calcium with silver, the size exclusion of ethane is responsible for this effect. An isosteric heat of ethylene adsorption of 95 kJ mol<sup>-1</sup> was reported in this work.

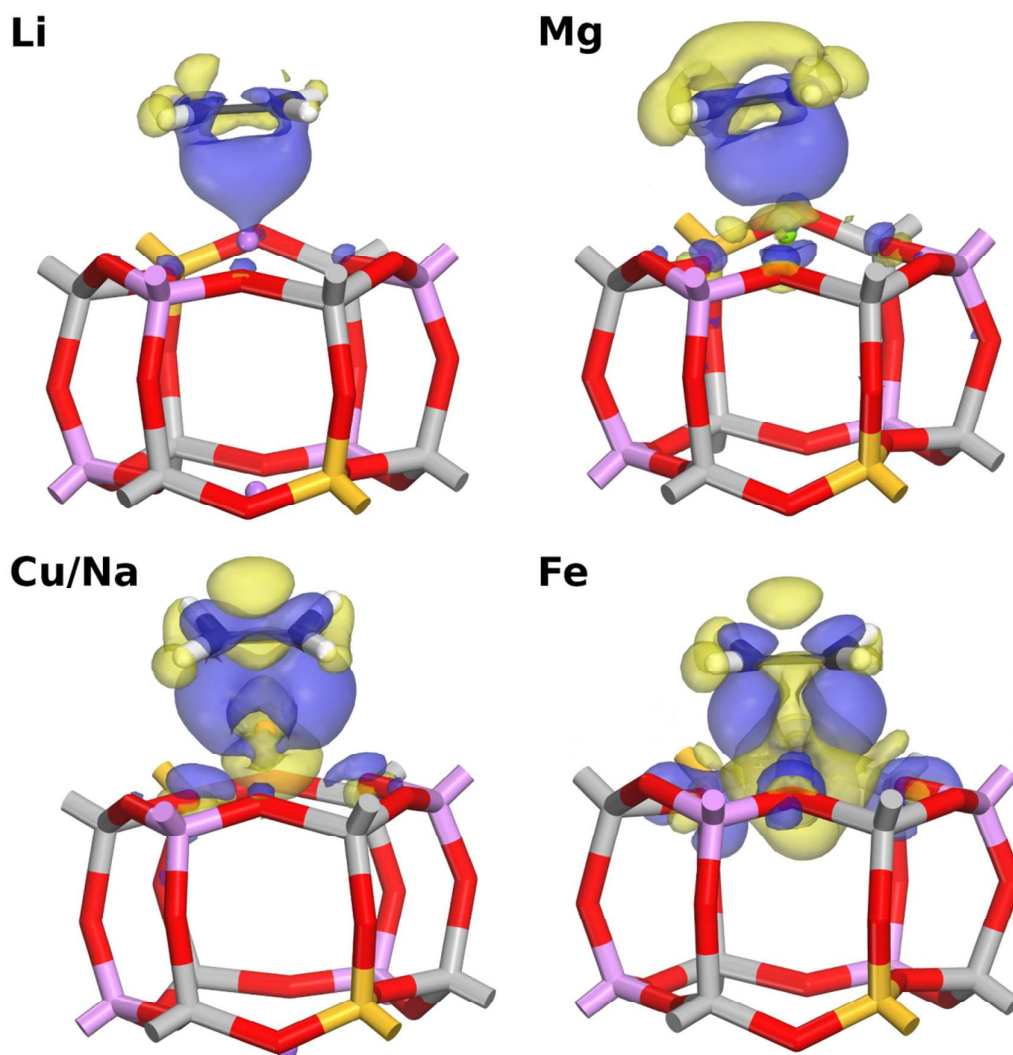


Figure 4: Isosurface of the electron density difference for ethylene adsorbed in Li-, Mg-, Cu/Na-, and Fe-SAPO-34. The colour scheme and the isodensity value are the same as in figure 3.

### Implications for the separation of hydrocarbon mixtures

As adsorption-based separation processes are based on the difference in affinity of the adsorbent towards the guest molecules involved, differences in isosteric heats of adsorption allow predictions to be made concerning the separation behaviour. The validity of this approach has been demonstrated, for example, using molecular simulations of CO<sub>2</sub>/N<sub>2</sub> mixture adsorption in MOFs.<sup>71</sup> As discussed above, the DFT interaction energy and the heat of adsorption are two conceptually different quantities. Nevertheless, it is reasonable to expect qualitative trends to be similar, allowing us to comment on the potential of the X-SAPO-34 systems for separations of binary mixtures involving the hydrocarbons considered. In this discussion, we focus on ethylene/ethane, propylene/propane, and ethylene/acetylene mixtures, due to their relevance for applications. The analysis uses the difference between the interaction energies obtained for a given pair of molecules as a measure of the difference in affinity: for example, high values of  $\Delta E_{int}(C_2H_4-C_2H_6)$  are interpreted as being indicative of a potentially high selectivity towards ethylene in the adsorption of an C<sub>2</sub>H<sub>4</sub>/C<sub>2</sub>H<sub>6</sub> mixture. The differences in interaction energy used in this analysis are visualised for the three mixtures in figure 5.

Among those adsorbents with main group cations, both  $\Delta E_{int}(C_2H_4-C_2H_6)$  and  $\Delta E_{int}(C_3H_6-C_3H_8)$  are largest for Mg-SAPO-34 (-30 kJ mol<sup>-1</sup> and -41 kJ mol<sup>-1</sup>), with Sr-SAPO-34 being the second-best system. This indicates that Mg-SAPO-34 could be a very interesting adsorbent for these separations. However, it must be kept in mind that the interaction in this system is predicted to be very strong, especially for propylene. This could make regeneration difficult, and thus Sr-SAPO-34 might be the more promising material if the absolute strength of the interactions were taken into account. Moreover, it has been shown that the adsorption properties of Sr-SAPO-34 can be optimised by varying the synthesis procedure,<sup>72</sup> whereas Mg-SAPO-34 exhibits only a modest adsorption performance, possibly due to limited accessibility of some pores in real samples.<sup>12</sup> While the energy differences obtained for alkene/alkane mixtures are appreciable, the difference in affinity between ethylene and acetylene is very small in all systems incorporating main group cations.

The adsorption behaviour seen in Mg-SAPO-34 is even more pronounced for the TM-exchanged systems. Here, ethylene and propylene are adsorbed much more strongly than ethane and propane, with energy differences ranging between -120 and -132 kJ mol<sup>-1</sup> in Cu/Na-SAPO-34 and Fe-SAPO-34, and around -80 kJ mol<sup>-1</sup> in Ag-SAPO-34. Obviously, such a large difference in affinity would be very favourable in terms of reaching a high selectivity, but again the strong interaction with the unsaturated species will be problematic when it comes to regeneration of the sorbent. It is very interesting to note that the SAPOs exchanged with different cations span a very wide range of values of  $\Delta E_{int}$ , which means that the adsorbent could be tailored with regard to the process conditions by using different cations. Furthermore, the TM-exchanged systems also exhibit moderate values of

$\Delta E_{int}(C_2H_4-C_2H_2)$ , reaching  $-22 \text{ kJ mol}^{-1}$  in Ag-SAPO-34. Thus, this material emerges as the most promising system for the separation of ethylene/acetylene mixtures.

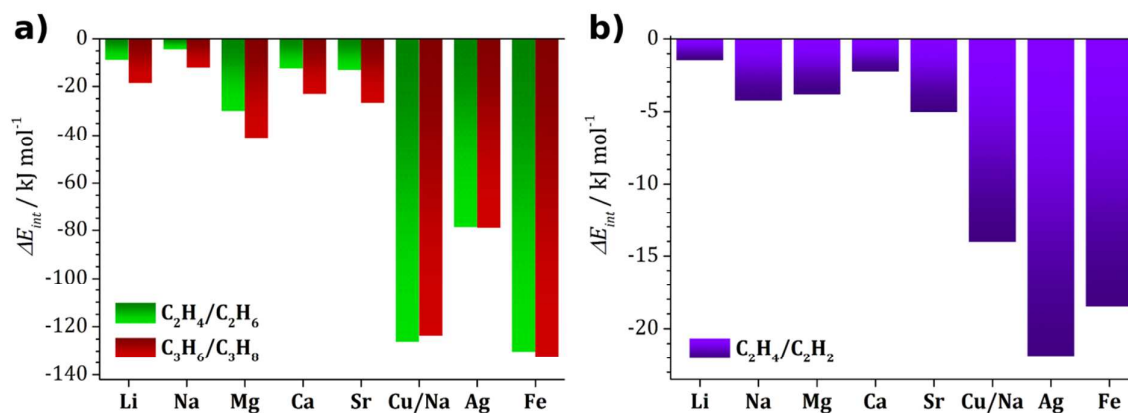


Figure 5: DFT interaction energy differences  $\Delta E_{int}$  for three different pairs of hydrocarbons: a) Ethylene/ethane and propylene/propane, b) ethylene/acetylene.

## Conclusions

We have used dispersion-corrected DFT calculations to predict the interaction of cation-exchanged SAPO-34 with saturated and unsaturated  $C_2$  and  $C_3$  hydrocarbons. An initial prediction of the preferred cation sites in SAPO-34 with a fixed Si/P ratio of 1:2 was performed to establish which cations are more stable at the SII site (associated with a six-ring), and which cations are preferred at the SIII' site (associated with an eight-ring). Among the ten cations considered, the largest monovalent cations potassium and rubidium are energetically preferred at the SIII' site, strontium constitutes a borderline case for which both sites are similar in energy, and all other cations are preferred at the SII site. A peculiar tendency of Cu cations to form strongly bonded dimers was observed, which is why one cation per d6R unit was replaced by sodium for this system.

In total, the following cations were considered in the calculations including guest molecules, the cation being located at the SII site:  $Li^+$ ,  $Na^+$ ,  $Mg^{2+}$ ,  $Ca^{2+}$ ,  $Sr^{2+}$ ,  $Cu^+$ ,  $Ag^+$ ,  $Fe^{2+}$ . All calculations used the semi-empirical dispersion correction developed by Grimme, and no vibrational effects were considered in the computation of the DFT-D interaction energies. While this is not the most sophisticated methodological approach, it allowed us to perform a large number of calculations for systems with different cations and different guest molecules. Carrying out the calculations within a consistent computational framework enabled us to make qualitative predictions regarding the trends in affinity. Using the difference between the interaction energies obtained for two molecules of interest

as a measure of the relative affinity, we were able to identify those systems that should hold most promise with regard to the separation of gas mixtures.

For the alkanes considered, the nature of the cation has only a moderate influence on the interaction strength. Although dispersive interactions are dominant, the electron density difference plots showed that there is a significant polarisation of the guest molecule. For unsaturated hydrocarbons, the systems with alkaline earth cations, particularly Mg-SAPO-34, provide a much stronger interaction than the alkali-exchanged SAPOs due to increased electrostatic and polarisation interactions. Due to large differences between the interaction energies obtained for unsaturated and saturated hydrocarbons, Mg-SAPO-34 or Sr-SAPO-34 could be promising systems for the separation of alkene/alkane mixtures. Strong interaction of the TM-exchanged SAPOs with unsaturated hydrocarbons was observed, with calculated interaction energies of up to  $-180 \text{ kJ mol}^{-1}$ . The short interatomic distances, as well as various features of the electron density difference, clearly point to an orbital-type interaction, which involves  $\sigma$ -donation and  $\pi$ -backdonation. This strong interaction is likely to render these systems unsuitable for adsorption-based separation processes involving unsaturated hydrocarbons, as it makes the regeneration very energy intensive. However, it should be emphasised that the suitability depends strongly on the process conditions – the TM-exchanged systems might be more interesting for separations carried out at higher temperatures, or for the removal of trace amounts of species like acetylene, where a high affinity towards the guest species could be more important than a particularly efficient regeneration. As such, the DFT-based predictions made in this work can provide only an initial assessment, and they should be followed by further computational and experimental studies that approach experimental conditions.

Finally, we briefly address the potential transferability of the results of this study to related systems. The calculations reported in this work considered only one type of SAPO, and looked at a fixed framework stoichiometry. Clearly, the total interaction energy obtained from analogous DFT calculations would change if a different topology was considered, or if the framework chemistry was modified (e.g. from SAPO to aluminosilicate). However, the strongly localised nature of the cation-guest interaction, particularly for unsaturated hydrocarbons, leads us to expect similar qualitative trends for other SAPOs and zeolites, at least for systems in which the cation is located in a comparable environment (i.e. at the centre of a six-ring). While comparable computational studies of hydrocarbon adsorption in other zeolites are lacking, previous works dealing with the adsorption of other molecules support the assumption of a relatively high degree of transferability: For the case of carbon monoxide, where the interaction with main-group cations is very localised due to the dominance of charge-dipole effects, a joint computational and experimental study has shown that the interaction energy varies only moderately (between  $-24$  and  $-36 \text{ kJ mol}^{-1}$ ) in Na-exchanged zeolites with different topologies, pore sizes, and Si/Al ratios.<sup>44</sup> Analogous observations were made for  $\text{CO}_2$  in

two K-exchanged zeolites with different topologies (FER and MFI), despite the increased importance of dispersion interactions for this guest molecule. Assuming a qualitatively similar behaviour for hydrocarbons, it can be expected that the main conclusions arising from this study should be valid not only for the specific case of SAPO-34, but also for a variety of related systems. There is thus reason to expect that our predictions regarding the suitability of zeolite-like materials exchanged with different cations for hydrocarbon separations will be transferable beyond the actual system studied.

### Acknowledgments

The authors acknowledge the use of the UCL Legion High Performance Computing Facility (Legion@UCL), and associated support services, in the completion of this work. M. Fischer acknowledges a postdoctoral fellowship by the German Research Foundation (DFG grant Fi 1800/1-1).

### Notes and references

Electronic Supplementary Information (ESI) available: Additional DFT results, visualisation of optimised geometries. See DOI: 10.1039/b000000x/

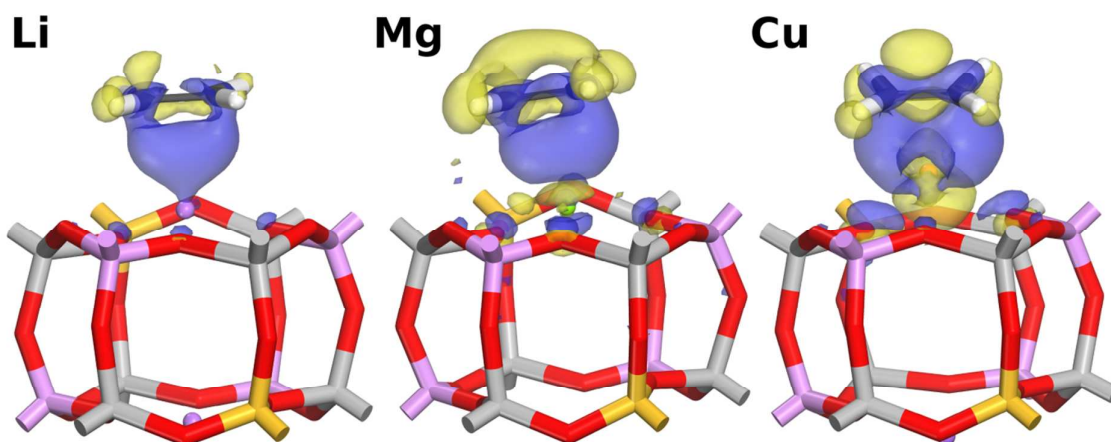
1. R. T. Yang, *Gas Separation by Adsorption Processes*, Imperial College Press, London, UK, 1997.
2. S. Choi, J. H. Drese, and C. W. Jones, *ChemSusChem*, 2009, **2**, 796–854.
3. Y.-S. Bae and R. Q. Snurr, *Angew. Chemie Int. Ed.*, 2011, **50**, 11586–11596.
4. D. M. Ruthven and S. C. Reyes, *Microporous Mesoporous Mater.*, 2007, **104**, 59–66.
5. S. Kulprathipanja, *Zeolites in Industrial Separation and Catalysis*, Wiley-VCH Verlag GmbH & Co. KGaA, Weinheim, Germany, 2010.
6. B. M. Lok, C. A. Messina, R. L. Patton, R. T. Gajek, T. R. Cannan, and E. M. Flanigen, *J. Am. Chem. Soc.*, 1984, **106**, 6092–6093.
7. J.-R. Li, J. Sculley, and H.-C. Zhou, *Chem. Rev.*, 2012, **112**, 869–932.
8. K. Sumida, D. L. Rogow, J. A. Mason, T. M. McDonald, E. D. Bloch, Z. R. Herm, T.-H. Bae, and J. R. Long, *Chem. Rev.*, 2012, **112**, 724–781.
9. Q. Liu, N. C. O. Cheung, A. E. Garcia-Bennett, and N. Hedin, *ChemSusChem*, 2011, **4**, 91–97.

10. O. Cheung, Q. Liu, Z. Bacsik, and N. Hedin, *Microporous Mesoporous Mater.*, 2012, **156**, 90–96.
11. M. E. Rivera-Ramos and A. J. Hernández-Maldonado, *Ind. Eng. Chem. Res.*, 2007, **46**, 4991–5002.
12. M. E. Rivera-Ramos, G. J. Ruiz-Mercado, and A. J. Hernández-Maldonado, *Ind. Eng. Chem. Res.*, 2008, **47**, 5602–5610.
13. M. Hong, S. Li, H. F. Funke, J. L. Falconer, and R. D. Noble, *Microporous Mesoporous Mater.*, 2007, **106**, 140–146.
14. S. R. Venna and M. A. Carreon, *Langmuir*, 2011, **27**, 2888–2894.
15. J. K. Das, N. Das, and S. Bandyopadhyay, *J. Mater. Chem. A*, 2013, **1**, 4966–4973.
16. W. Zhu, F. Kapteijn, and J. A. Moulijn, *Chem. Commun.*, 1999, 2453–2454.
17. D. H. Olson, M. A. Cambor, L. A. Villaescusa, and G. H. Kuehl, *Microporous Mesoporous Mater.*, 2004, **67**, 27–33.
18. M. Palomino, A. Cantín, A. Corma, S. Leiva, F. Rey, and S. Valencia, *Chem. Commun.*, 2007, 1233–1235.
19. M. Khalighi, Y. F. Chen, S. Farooq, I. A. Karimi, and J. W. Jiang, *Ind. Eng. Chem. Res.*, 2013, **52**, 3877–3892.
20. K. Agarwal, M. John, S. Pai, B. L. Newalkar, R. Bhargava, and N. V. Choudary, *Microporous Mesoporous Mater.*, 2010, **132**, 311–318.
21. G. Aguilar-Armenta and M. E. Patiño-Iglesias, *Langmuir*, 2002, **18**, 7456–7461.
22. A. van Miltenburg, J. Gascon, W. Zhu, F. Kapteijn, and J. A. Moulijn, *Adsorption*, 2008, **14**, 309–321.
23. S. Aguado, G. Bergeret, C. Daniel, and D. Farrusseng, *J. Am. Chem. Soc.*, 2012, **134**, 14635–14637.
24. J. Padin and R. T. Yang, *Ind. Eng. Chem. Res.*, 1997, **36**, 4224–4230.
25. R. T. Yang, *Adsorbents: Fundamentals and Applications*, John Wiley & Sons, Inc, Hoboken, New Jersey, USA, 1st edn., 2003.
26. C. A. Grande, J. D. P. Araujo, S. Cavenati, N. Firpo, E. Basaldella, and A. E. Rodrigues, *Langmuir*, 2004, **20**, 5291–5297.
27. N. Lamia, M. Jorge, M. A. Granato, F. A. Almeida Paz, H. Chevreau, and A. E. Rodrigues, *Chem. Eng. Sci.*, 2009, **64**, 3246–3259.
28. M. Fischer, J. R. B. Gomes, M. Fröba, and M. Jorge, *Langmuir*, 2012, **28**, 8537–8549.
29. E. D. Bloch, W. L. Queen, R. Krishna, J. M. Zadrozny, C. M. Brown, and J. R. Long, *Science*, 2012, **335**, 1606–1610.

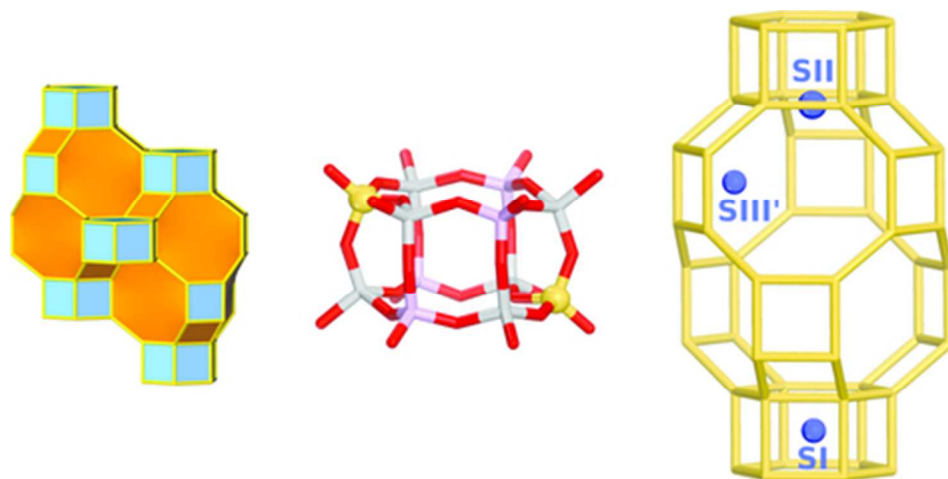
30. Z. R. Herm, E. D. Bloch, and J. R. Long, *Chem. Mater.*, 2014, **26**, 323–338.
31. J. Kim, M. Abouelnasr, L.-C. Lin, and B. Smit, *J. Am. Chem. Soc.*, 2013, **135**, 7545–7552.
32. J. Kim, L.-C. Lin, R. L. Martin, J. A. Swisher, M. Haranczyk, and B. Smit, *Langmuir*, 2012, **28**, 11914–11919.
33. M. Fischer and R. G. Bell, *J. Phys. Chem. C*, 2012, **116**, 26449–26463.
34. M. Fischer and R. G. Bell, *J. Phys. Chem. C*, 2013, **117**, 17099–17110.
35. F. Götzl and J. Hafner, *J. Chem. Phys.*, 2011, **134**, 064102.
36. F. Götzl, A. Grüneis, T. Buciko, and J. Hafner, *J. Chem. Phys.*, 2012, **137**, 114111.
37. G. Hübner, G. Rauhut, H. Stoll, and E. Roduner, *Phys. Chem. Chem. Phys.*, 2002, **4**, 3112–3121.
38. G. Hübner, G. Rauhut, H. Stoll, and E. Roduner, *J. Phys. Chem. B*, 2003, **107**, 8568–8573.
39. P. Rejmak, M. Mitoraj, and E. Broclawik, *Phys. Chem. Chem. Phys.*, 2010, **12**, 2321–2330.
40. E. Broclawik, J. Załucka, P. Kozyra, M. Mitoraj, and J. Datka, *J. Phys. Chem. C*, 2010, **114**, 9808–9816.
41. S. J. Clark, M. D. Segall, C. J. Pickard, P. J. Hasnip, M. I. J. Probert, K. Refson, and M. C. Payne, *Z. Kristallogr.*, 2005, **220**, 567–570.
42. J. P. Perdew, K. Burke, and M. Ernzerhof, *Phys. Rev. Lett.*, 1996, **77**, 3865–3868.
43. S. Grimme, *J. Comput. Chem.*, 2006, **27**, 1787–1799.
44. P. Nachtigall, M. R. Delgado, D. Nachtigallova, and C. O. Areal, *Phys. Chem. Chem. Phys.*, 2012, **14**, 1552–1569.
45. E. R. Johnson, I. D. Mackie, and G. A. DiLabio, *J. Phys. Org. Chem.*, 2009, **22**, 1127–1135.
46. F. Hanke, *J. Comput. Chem.*, 2011, **32**, 1424–1430.
47. L. Leardini, S. Quartieri, and G. Vezzalini, *Microporous Mesoporous Mater.*, 2010, **127**, 219–227.
48. M. Zokaie, U. Olsbye, K. P. Lillerud, and O. Swang, *J. Phys. Chem. C*, 2012, **116**, 7255–7259.
49. L. J. Smith, H. Eckert, and A. K. Cheetham, *J. Am. Chem. Soc.*, 2000, **122**, 1700–1708.
50. B. Civalleri, A. Ferrari, M. Lluell, R. Orlando, M. Merawa, and P. Ugliengo, *Chem. Mater.*, 2003, **15**, 3996–4004.
51. R. D. Shannon, *Acta Crystallogr. Sect. A*, 1976, **32**, 751–767.
52. L. J. Smith, H. Eckert, and A. K. Cheetham, *Chem. Mater.*, 2001, **13**, 385–391.

53. W. J. Mortier, *Compilation of extra-framework sites in zeolites*, Butterworth Scientific Limited, Guildford, Surrey, UK, 1982.
54. M. Fischer and R. G. Bell, *Zeitschrift für Krist. - Cryst. Mater.*, 2013, **228**, 124–133.
55. M. Calligaris, A. Mezzetti, G. Nardin, and L. Randaccio, *Zeolites*, 1984, **4**, 323–328.
56. G. Moretti, G. Ferraris, G. Fierro, M. Jacono, S. Morpurgo, and M. Faticanti, *J. Catal.*, 2005, **232**, 476–487.
57. S. Morpurgo, G. Moretti, and M. Bossa, *Phys. Chem. Chem. Phys.*, 2007, **9**, 417–424.
58. M. R. Hudson, W. L. Queen, J. A. Mason, D. W. Fickel, R. F. Lobo, and C. M. Brown, *J. Am. Chem. Soc.*, 2012, **134**, 1970–1973.
59. D. W. Fickel and R. F. Lobo, *J. Phys. Chem. C*, 2010, **114**, 1633–1640.
60. F. Göttl, R. E. Bulo, J. Hafner, and P. Sautet, *J. Phys. Chem. Lett.*, 2013, **4**, 2244–2249.
61. F. Giordanino, P. N. R. Vennestrøm, L. F. Lundegaard, F. N. Stappen, S. Mossin, P. Beato, S. Bordiga, and C. Lamberti, *Dalton Trans.*, 2013, **42**, 12741–12761.
62. A. Pulido, P. Nachtigall, A. Zukal, I. Domínguez, and J. Čejka, *J. Phys. Chem. C*, 2009, **113**, 2928–2935.
63. G. D. Pirngruber, P. Raybaud, Y. Belmabkhout, J. Čejka, and A. Zukal, *Phys. Chem. Chem. Phys.*, 2010, **12**, 13534–13546.
64. J. F. M. Denayer, L. I. Devriese, S. Couck, J. Martens, R. Singh, P. A. Webley, and G. V. Baron, *J. Phys. Chem. C*, 2008, **112**, 16593–16599.
65. R. D. Johnson (Editor), *NIST Comput. Chem. Comp. Benchmark Database, NIST Stand. Ref. Database Number 101*, 2013.
66. E. Cubero, F. J. Luque, and M. Orozco, *Proc. Natl. Acad. Sci. U. S. A.*, 1998, **95**, 5976–5980.
67. A. S. Mahadevi and G. N. Sastry, *Chem. Rev.*, 2013, **113**, 2100–2138.
68. M. S. Nechaev, V. M. Rayón, and G. Frenking, *J. Phys. Chem. A*, 2004, **108**, 3134–3142.
69. A. G. Bezus, A. V. Kiselev, Z. Sedlacek, and P. Q. Du, *Trans. Faraday Soc.*, 1971, **67**, 468–482.
70. T. G. Andronikashvili, G. V. Tsitsishvili, and L. Y. Laperashvili, *Chromatographia*, 1975, **8**, 223–227.
71. D. Wu, Q. Yang, C. Zhong, D. Liu, H. Huang, W. Zhang, and G. Maurin, *Langmuir*, 2012, **28**, 12094–12099.
72. A. G. Arévalo-Hidalgo, N. E. Almodóvar-Arbelo, and A. J. Hernández-Maldonado, *Ind. Eng. Chem. Res.*, 2011, **50**, 10259–10269.

## Table of Contents figure



The interaction of  $C_2$  and  $C_3$  hydrocarbons with cation-exchanged SAPO-34 materials is studied using DFT-D calculations, permitting predictions regarding their suitability for alkene/alkane separations.



39x19mm (300 x 300 DPI)